Including the nonlinear response of neurons to improve the prediction of visual acuity across levels of contrast, luminance, and blur

Charles-Edouard Leroux, Christophe Fontvieille, Fabrice Bardin

Vision Research 234 (2025) 108652

Contents lists available at ScienceDirect

Vision Research

journal homepage: www.elsevier.com/locate/visres

Including the nonlinear response of neurons to improve the prediction of visual acuity across levels of contrast, luminance, and blur

Charles-Edouard Leroux *, Christophe Fontvieille, Fabrice Bardin

Laboratoire MIPA, Université de Nîmes, France

ARTICLE INFO

Keywords:
Acuity model
Letter identification
Wave optics
Decision theory
Neural images

ABSTRACT

We present a theoretical model that predicts visual acuity changes over extended ranges of stimulus contrast, luminance, and optical blur. We highlight the significance of neuronal response nonlinearity to optical contrast in achieving model agreement with experimental data. The model operates by computing, for each experimental condition, a parameter termed *data separability* within the framework of statistical decision theory. We assume a theoretical model observer that utilizes sharp image templates for optotype identification, consistent with our previous work for small (< 0.5 D) optical aberrations (Leroux et al., 2024). The model incorporates the nonlinear response of visual neurons to contrast stimuli in the simulation of visual images. We digitalized measurements from Johnson and Casson (1995), who studied the combined effects of stimulus contrast (6 to 97%), luminance (0.075 to 75 cd/m^2), and blur (0 to 8 D positive lens), and compared our model's predictions to their data. The model achieved an overall root-mean-square residual of 0.048 logMAR for measurements spanning 1.73 logMAR. Accounting for nonlinearity proved critical in predicting acuity across these extended ranges of experimental conditions. This approach may also be necessary for modeling acuity under non-standard experimental conditions and/or for subjects with pathologies.

1. Introduction

Visual neurons exhibit nonlinear responses to optical contrast. Nonlinearity in neuronal electrical responses has been observed *in vivo* in the retina (Scholl, Latimer, & Priebe, 2012), the lateral geniculate nucleus (Duong & Freeman, 2008), and the primary visual cortex (Albrecht & Hamilton, 1982). The response is expansive at low contrast and compressive at high contrast. Additionally, the sensitivity of a neuron is diminished when neighboring neurons within its suppressive field are exposed to high optical contrast (Carandini & Heeger, 1994; Carandini, Heeger, & Movshon, 1997).

Models of spatial vision that incorporate neuronal nonlinearity effectively predict contrast sensitivity measurements in pattern masking experiments (Watson & Solomon, 1997). However, contrast sensitivity (Watson & Ahumada, 2005, 2015) and visual acuity (Nestares, Navarro, & Antona, 2003; Watson & Ahumada, 2008, 2012) measurements can be accurately modeled without considering neuronal nonlinearity. We hypothesize that acuity models spanning broader experimental ranges should account for neuronal nonlinearity.

One fundamental challenge in spatial vision is to quantify optical and neural factors affecting visual performance over broad ranges of stimulus contrast, luminance, and optical blur, within populations of subjects (Applegate, Marsack, & Thibos, 2006; Pesudovs, Marsack, Donnelly, Thibos, & Applegate, 2004; Villegas, Alcón, & Artal, 2008) or at the level of a single subject (Dalimier, Dainty, & Barbur, 2008; Marcos, Sawides, Gambra, & Dorronsoro, 2008). From the clinical perspective, there are diagnostic advantages of combining visual acuity measurements under varying contrast (Baier et al., 2005) and luminance (Wood, Jolly, Buckley, Josan, & MacLaren, 2021) conditions for identifying ocular pathologies.

Simple acuity models that use few degrees of freedom are essential tools for analyzing clinical data. Studies investigating the relationship between visual performance and the monochromatic aberrations of the eye often rely on visual image quality metrics (Guirao & Williams, 2003; Thibos, Hong, Bradley, & Applegate, 2004) as simplified representations of visual acuity, expressed as single values derived from wavefront maps. Metrics predict the effects of monochromatic aberrations on objective refraction (Kilintari, Pallikaris, Tsiklis, & Ginis, 2010; Martin, Vasudevan, Himebaugh, Bradley, & Thibos, 2011), on depth of focus (Yi, Iskander, & Collins, 2011; Zheleznyak, Jung, & Yoon, 2014; Zheleznyak, Sabesan, Oh, MacRae, & Yoon, 2013), and on accommodation (Buehren & Collins, 2006; López-Gil, Martin, Liu, Bradley, Díaz-Muñoz, & Thibos, 2013; Tarrant, Roorda, & Wildsoet,

* Corresponding author.
E-mail addresses: charles.leroux@unimes.fr (C.-E. Leroux), christophe.fontvieille@unimes.fr (C. Fontvieille), fabrice.bardin@unimes.fr (F. Bardin).

https://doi.org/10.1016/j.visres.2025.108652
Received 4 February 2025; Received in revised form 9 May 2025; Accepted 3 June 2025

2010). Metrics do not take account of key stimulus properties, such as contrast, to predict visual acuity. As a more complex approach, Monte Carlo models involve the complete simulation of noise-corrupted visual images and their subsequent identification by the subject.

To circumvent the computational complexity of Monte Carlo methods, we employed the concept of *data separability*, rooted in statistical decision theory, to predict relative changes in visual acuity across a narrow range (< 0.5 D) of optical blur (Leroux, Leahy, Dupuis, Fontvieille, & Bardin, 2024). Calculating data separability is significantly less computationally demanding than implementing Monte Carlo models. This approach only requires the simulation of noise-free visual images. In this study, we evaluated the potential of this simple approach by incorporating the nonlinearity of neuronal responses to optical contrast. Our objective was to predict visual acuity measurements with a four-orientation Landolt C test, as reported by Johnson and Casson (1995), over extended ranges of contrast, luminance, and dioptric blur.

2. Methods

2.1. Experimental data

The data presented in Figures 1, 3, and 5 of Johnson and Casson (1995) were extracted using dedicated software (PlotDigitizer, https://plotdigitizer.com). We referred to these data sets as *Data 1*, *Data 3*, and *Data 5*, respectively. *Data 1* consisted of 97% contrast visual acuity measurements obtained using positive lenses (ranging from 0 D to +8 D in 1 D steps) under various luminance levels (75, 7.5, 0.75, and 0.075 cd/m^2). *Data 3* consisted of high luminance (75 cd/m^2) visual acuity measurements obtained using the same range of positive lenses and varying levels of stimulus contrast (97, 48.5, 24, 12, and 6% Michelson contrast). *Data 5* consisted of visual acuity measurements at different combinations of stimulus contrast (97, 48.5, 24, 12, and 6% Michelson contrast) and luminance (75, 7.5, 0.75, and 0.075 cd/m^2), with no additional lens applied to the subject's refractive correction.

The digitalization accuracy was better than ±0.01 logMAR (a fraction of the graphic markers in Johnson and Casson's article). The error bars reported by Johnson and Casson, which represented inter-subject variability, ranged from ±0.03 logMAR to ±0.1 logMAR depending on the experimental condition. Only the subject-averaged measurements were digitalized. Each measurement represented the mean acuity of four subjects (mean age: 35) and was obtained using the Landolt C optotype and a four-alternative forced choice orientation test (i.e., the gap pointing up, down, left, or right), as described in Johnson and Casson's study.

2.2. Computation of data separability

Building on our recent work (Leroux et al., 2024), we predicted visual acuity measurements by computing, for each experimental condition, *data separability* as a function of optotype size (a, the angular extent of the Landolt C's gap). Data separability is an extension of the d' measure of separability, adapted for classification tasks involving more than two classes of stimuli (Barrett & Myers, 2003, p.819–852). Data separability is an estimate of the signal-to-noise ratio of the test statistics used by a model observer to classify the orientation of the Landolt C. The model observer considered in this paper utilized a blur-free image template of the stimulus for identification and was referred to as the *real observer* in our previous work (Leroux et al., 2024). This template image was defined as a spatial function of luminance, $O_{k,a}(x,y)$, where the index k represents the orientation of the Landolt C, the feature to be identified. According to statistical decision theory, data separability (S) remains constant at the size threshold that defines visual acuity across all experimental conditions. This constant value directly relates to the percentage of correct responses in restricted examples of classification tasks, particularly in tasks involving only two classes. Larger threshold sizes are required to preserve data separability in the presence of optical blur, low stimulus contrast, and/or low luminance. Data separability S was computed as the sum (over $k = 1$ to 4 possible orientations) of the scalar products between the differences in the visual image, $\Delta I_{k,a}(x,y)$, and the differences in the template image, $\Delta O_{k,a}(x,y)$:

$$S(a) = \frac{1}{\sigma}\sqrt{\sum_{k=1}^{4}\frac{\left(\iint \Delta I_{k,a}(x,y)\Delta O_{k,a}(x,y)dxdy\right)^2}{\iint \Delta O_{k,a}^2(x,y)dxdy}} \quad (1)$$

Here, Δ denotes the difference between an image $I_{k,a}(x,y)$ (corresponding to orientation k) and the orientation-averaged image: $\Delta I_{k,a}(x,y) = I_{k,a}(x,y) - \frac{1}{4}\sum_{i=1}^{4} I_{i,a}(x,y)$. The same notation applies to $\Delta O_{k,a}(x,y)$. σ is the standard deviation of the assumed white noise in the visual images. It was set to an arbitrary value of 1 throughout the paper, because the measurement of visual acuity under the reference condition defined the reference value S_0 (see Section 2.4).

2.3. Simulation of visual images

In our previous work, we simulated visual images $I_{k,a}(x,y)$ as the convolution between the object ($O_{k,a}(x,y)$, identical to the template function) with the visual point spread function $h(x,y)$. The latter was calculated as the inverse Fourier transform of the product between the Optical Transfer Function (OTF) and the Neural Transfer Function (NTF). Using this linear approximation, data separability (S) is proportional to Weber stimulus contrast (Dalimier & Dainty, 2008) and remains unchanged with respect to contrast polarity.

In this study, we introduced a nonlinear mapping to transform visual images. This approach follows the modeling methodology used for predicting pattern-masking experiments (Watson & Solomon, 1997), which involves the sequential application of linear filters first (via the OTF and the NTF) followed by a nonlinear transformation. The Naka-Rushton function f, widely used to model the electrical responses of visual neurons to optical contrast (Albrecht & Hamilton, 1982), was expressed as:

$$f(c) = \frac{c^n}{c^n + c_{50}^n} \quad (2)$$

f is a function of the contrast (c) of the visual image. It is parameterized by the exponent n and the input contrast c_{50} for which the output contrast is 50%. The nonlinear function f can include additional degrees of freedom for scale and offset (Rathbun, Alitto, Warland, & Usrey, 2016). However, these parameters were omitted in this work, as they do not influence the predicted value of visual acuity values based on data separability. We show in Fig. 1A the f function with parameters $n = 2$ and $c_{50} = 0.3$, which are typical values in the literature (Duong & Freeman, 2008; Rathbun et al., 2016).

The simulated visual images $I_{k,a}(x,y)$ were computed as:

$$I_{k,a}(x,y) = f(h(x,y) * O_{k,a}(x,y)) \quad (3)$$

The OTF was computed for each level of blur and luminance. We used the formula of Watson and Yellott (2012) to estimate pupil diameter based on the luminance levels and experimental parameters reported by Johnson and Casson (1995): binocular viewing of a 2.9 ° visual field and an average subject age of 35 years. The estimated pupil diameters were as follows: 5.9 mm at 75 cd/m^2, 6.5 mm at 7.5 cd/m^2, 7.1 mm at 0.75 cd/m^2, and 7.3 mm at 0.075 cd/m^2. In addition to the optical blur introduced by the lens in the Johnson and Casson study, we accounted for monochromatic aberrations using the model derived by Thibos (2009). The generalized pupil function was initially computed for a 7.5 mm diameter and resized to match the pupil diameters provided by Watson's formula. The OTF was then calculated as the average OTF from 100 model eyes. Longitudinal and transversal chromatic aberrations were neglected in our model, as they have negligible effects on visual performance when monochromatic aberrations are uncorrected (Roorda et al., 2023).

The NTF was computed using the MATLAB code provided by Hastings, Marsack, Thibos, and Applegate (2020), using as input parameters the subjects' average age (35 years) and the estimated retinal illuminance (i.e., luminance × pupil area, in Trolands) for each experimental condition. We have multiplied the NTFs of reduced luminance with three parameters (α_1 at 7.5 cd/m^2, α_2 at 0.75 cd/m^2, α_3 at 0.075 cd/m^2) that were optimized to fit measurements (see Section 2.5). We did not rescale the NTF at the highest luminance level (75 cd/m^2), because it would not influence the predicted value of visual acuity. Indeed, as detailed in Section 2.4, the model prediction is based on a reference condition at 75 cd/m^2 luminance level. The NTFs, as computed by the code provided by Hastings et al. (2020), are shown in Fig. 1B, for the four luminance levels of the Johnson and Casson study. We propose two justifications for rescaling the NTFs under reduced luminance: first, the literature on NTF measurements exhibits substantial variability; second, these measurements are likely influenced by nonlinear detection of grating contrast, thereby rendering their direct use in modeling the linear stage of visual image formation prone to error.

2.4. Model prediction of acuity

Fig. 1C illustrates how we computed the model's prediction of visual acuity using the principle of equal data separability. We first computed data separability S as a function of letter size for the reference condition of high contrast (97%), high luminance (75 cd/m^2), and no blur (solid blue line). We estimated the reference value (S_0) of data separability that corresponded to the acuity measurement in this reference condition (−0.06 logMAR, see dashed line). In Fig. 1C, the reference value is $S_0 = 0.11$ (horizontal dashed black line). To predict visual acuity in any other experimental condition, we computed the corresponding data separability as a function of letter size. We then estimated the letter size for which data separability equaled the S_0 reference value. We show an example in Fig. 1C, for the condition of 6% contrast, 75 cd/m^2 luminance, and no blur: solid yellow line. The predicted logarithm of letter size is 0.55 logMAR. In Fig. 1C, we have used $n = 2$, $c_{50} = 0.3$, $[\alpha_1, \alpha_2, \alpha_3] = [1, 1, 1]$.

2.5. Fitting parameters

Unless otherwise specified, we used $N = 5$ fit parameters (n, c_{50}, α_1, α_2, α_3) to optimize the model's predictions, using the MATLAB built-in function *lsqnonlin*. The root-mean-square (RMS) residual (model – measurement, in logMAR units) was used as the figure of merit for the optimization process. To highlight the significance of the nonlinear response of visual neurons to contrast, we evaluated the RMS residual as a function of the number N of fit parameters.

For $N = 0$, we assumed a linear neuronal response, replacing f with the identity function in Eq. (3). In this case, the NTFs of Hastings et al. (2020) were not rescaled ($[\alpha_1, \alpha_2, \alpha_3] = [1, 1, 1]$).

For $N = 3$, the neuronal response remained linear, but we rescaled the model NTFs with the α_1, α_2, and α_3 fit parameters.

For $N = 5$, the model incorporated the nonlinearity of the neuronal response, fitting all five parameters (n, c_{50}, α_1, α_2, α_3) to minimize the RMS residual.

We performed a likelihood-ratio test, which consisted of computing the probability p of observing the fit improvement brought by the two additional parameters (n and c_{50}) by chance. To this end, we computed the log-likelihood of observing the Carson and Johnson measurements for each modeling approach ($N = 3$ and $N = 5$), assuming that they follow independent Gaussian distributions with equal standard deviations of Σ and means equal to the corresponding model predictions. Under this assumption, the log-likelihood of each model was given by $nRMS^2/2\Sigma^2$, where $n = 78$ was the number of measurement conditions. Using Wilks' theorem, we computed the p-value of the likelihood-ratio test as the upper-tail probability from the χ^2 distribution with two degrees of freedom (the difference in the number of model parameters), evaluated at twice the log-likelihood difference between the two models.

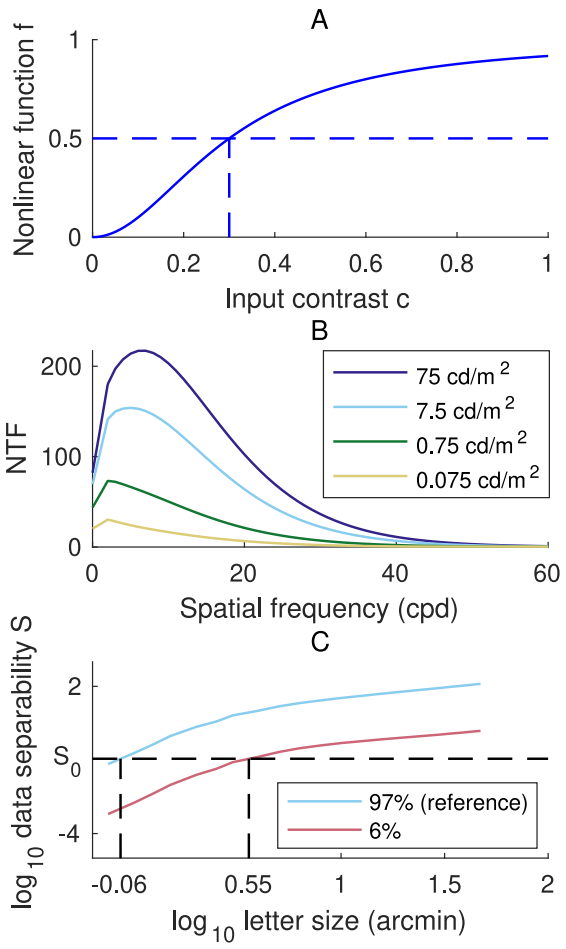

Fig. 1. (A) Naka-Rushton nonlinearity function $f(c)$, which describes the neuronal response to optical contrast with parameters $n = 2$ and $c_{50} = 0.3$. (B) Neural transfer functions (NTF) at the different luminance levels, computed in dimensionless units using the code provided by Hastings et al. (2020). (C) Data separability S, as a function of the logarithm of letter size a. The measured acuity in the reference condition is −0.06 logMAR. The corresponding value of data separability in the reference condition is S_0. For any other condition (for example 6% contrast, solid red line), we computed a model acuity as the letter size for which data separability equaled S_0 (here 0.55 logMAR).

3. Results

Figs. 2A–C show visual acuity measurements from the Johnson and Casson study (circle markers, logMAR units) and predictions from our model (solid lines). These predictions incorporated the $N = 5$ fitted parameters described in the Methods section. Each subfigure corresponds to a specific experimental condition. Fig. 2A shows visual acuity as a function of optical blur under varying luminance levels (*Data 1*). Fig. 2B shows visual acuity as a function of optical blur at different stimulus contrasts (*Data 3*). Fig. 2C shows visual acuity as a function of stimulus contrast under varying luminance levels (*Data 5*).

Fig. 2D shows the histogram of residuals (model predictions – measurements) for the combined datasets, using $N = 5$ fitted parameters. Residuals followed a Gaussian distribution, confirmed by the Shapiro–Wilk test ($p = 0.4$), with an overall RMS residual of 0.048 logMAR. Residuals for individual datasets were similarly distributed, with RMS values of 0.042, 0.049, and 0.045 logMAR for *Data 1*, *Data 3*, and *Data 5*, respectively.

Fig. 3A shows the RMS residual as a function of the number N of fit parameters (see Methods). For $N = 0$ (no fit parameters), RMS = 0.24 logMAR. For $N = 3$, the optimized fit parameters were $[\alpha_1, \alpha_2, \alpha_3] = [0.21, 0.15, 0.16]$, and RMS = 0.18 logMAR. For $N = 5$, the optimized

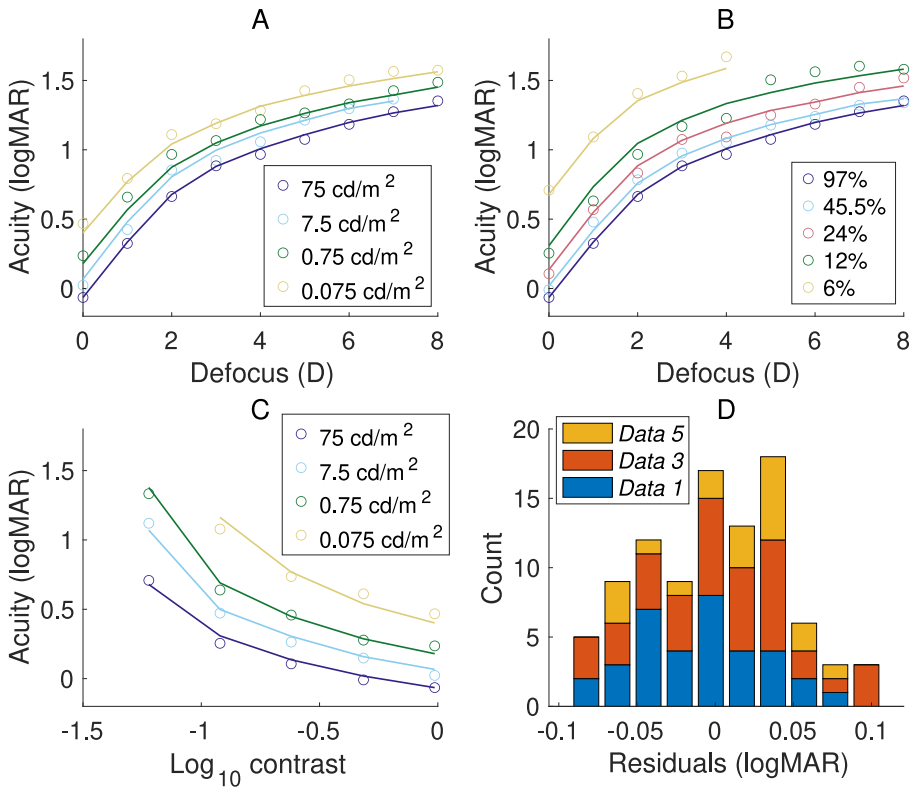

Fig. 2. Comparison of model predictions and experimental measurements of visual acuity. (A–C) Visual acuity (in logMAR) as a function of: (A) Optical blur across luminance levels (75, 7.5, 0.75, 0.075 cd/m^2, *Data 1*). (B) Optical blur across stimulus contrast levels (97%, 48.5%, 24%, 12%, and 6%, *Data 3*). (C) Stimulus contrast across luminance levels (*Data 5*). Solid lines represent model predictions, and circle markers denote measurements from Johnson and Casson (1995). (D) Histograms of residuals (model prediction minus measurement) for all datasets (blue: *Data 1*, red: *Data 3*, yellow: *Data 5*). Residuals followed a Gaussian distribution (Shapiro–Wilk test, $p = 0.4$) with a root-mean-square residual of 0.048 logMAR.

fit parameters were $c_{50} = 0.36$, $n = 2.61$, $[\alpha_1, \alpha_2, \alpha_3] = [0.85, 1.24, 1.47]$, and RMS = 0.048 logMAR. The inclusion of neuronal nonlinearity ($N = 5$) significantly improved model predictions compared to $N = 3$, as confirmed by the log-likelihood test ($p < 0.000001$ assuming a measurement standard deviation of $\Sigma < 0.3$ logMAR).

Without neuronal nonlinearity ($N = 3$), the $[\alpha_1, \alpha_2, \alpha_3]$ parameters are optimized to very small values to model the measured acuity loss with decreasing luminance. With neuronal nonlinearity ($N = 5$), however, these parameters need not to be as small, as the nonlinearity enhances the impact of a reduced NTF under low luminance conditions.

Figs. 3B and 3C compare the model's performance with and without nonlinearity (solid and dashed lines, respectively) under various conditions. Measurements (circle markers) and model predictions are shown as functions of the logarithm of stimulus contrast (Fig. 3B, subset of *Data 3*) and luminance (Fig. 3C, subset of *Data 1* and *Data 5*). In Fig. 3B, the significant acuity loss at low stimulus contrast was predicted only when neuronal nonlinearity was accounted for. In Fig. 3C, without neuronal nonlinearity, the model overestimates acuity loss at high stimulus contrast and underestimates it at low stimulus contrast. When neuronal nonlinearity is included, the decrease in acuity with luminance is accurately modeled at both levels of stimulus contrast.

4. Discussion

We present a model that predicts visual acuity measurements across an extended range of experimental conditions. Nonlinearity was found to have a significant influence on model agreement. Overall, we obtained good model agreement (RMS residual = 0.048 logMAR, with $N = 5$ fit parameters) for acuity measurements spanning 1.7 logMAR. The linear model without fit parameters, as previously presented by Leroux et al. (2024) under fixed stimulus contrast and luminance, performed poorly in predicting measurements (RMS residual = 0.24 logMAR, with $N = 0$ fit parameter). We initially attempted to improve it by scaling NTFs at each luminance level using the $[\alpha_1, \alpha_2, \alpha_3]$ fit parameters; however, it failed to predict measurements accurately (RMS residual = 0.18 logMAR, with $N = 3$ fit parameter). Moreover, the optimized scaling parameters ($\alpha_{1,2,3} \approx 0.2$) significantly differed from unity, indicating apparent disagreement with the NTF models of Hastings et al. (2020). Indeed, the NTF models at 7.5 cd/m^2 and below were rescaled by a factor of ≈ 0.2 to minimize the RMS residual, while the NTF model at 75 cd/m^2 was not rescaled, as it corresponded to the reference condition of our acuity model. By introducing two additional fit parameters (n and c_{50}) to model neuronal nonlinearity, the RMS was significantly reduced to 0.048 logMAR. The optimized $[\alpha_1, \alpha_2, \alpha_3]$ values approached unity, aligning with the NTF models of Hastings et al. (2020).

The optimized values of the nonlinear parameters ($n = 2.61$ and $c_{50} = 0.36$) were comparable to the direct measurements of neuronal responses in the lateral geniculate nucleus (Duong & Freeman, 2008, $n = 2.03$ and $c_{50} = 0.3887$, median of 168 cells) and in the primary visual cortex (Albrecht & Hamilton, 1982, $n = 2.9$ and $c_{50} = 0.193$, mean of 225 cells). We should compare these values cautiously for several reasons. Direct measurements vary widely between cells of the same type, which are tuned to reduced ranges of input contrast, and our optimized values relates to an overall contrast response function. This function is likely to saturate at lower stimulus contrast than the average function of individual cells because it reaches saturation when the most sensitive cells do. This collective effect is readily observed when comparing the contrast response of a cell in the lateral geniculate nucleus to the response of the two to five retinal cells from which this response originates (Rathbun et al., 2016). Direct measurements of individual cells are reported as functions of the contrast displayed by the monitor. In our model, we follow the approach introduced

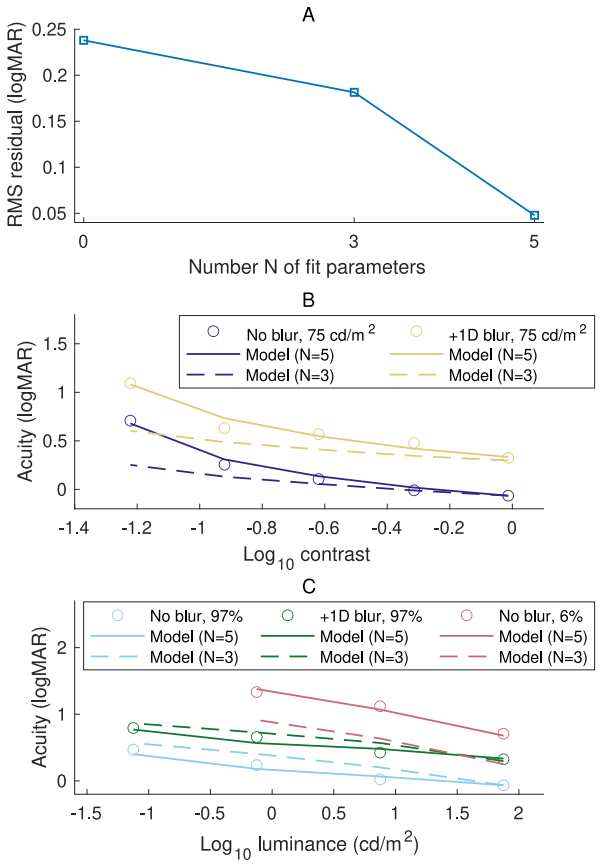

Fig. 3. (A) Root-mean-square (RMS) residual (in logMAR), as a function of the number of fit parameters (N). $N = 0$ corresponds to the model with no fit parameters (the neuronal response to contrast is linear and the neural transfer functions (NTF) are directly computed by the program of Hastings et al., 2020). For $N = 3$, fit parameters (α_1, α_2, α_3) scale the NTFs at different levels of luminance. For $N = 5$, fit parameters (c_{50}, n, α_1, α_2, α_3) also accounts for the nonlinearity of the neuronal response. (B and C) Measurements (circles) and model predictions of visual acuity (solid lines: with neuronal nonlinearity, $N = 5$ fit parameters; dashed lines: without neuronal nonlinearity, $N = 3$ fit parameters) as functions of logarithm of stimulus contrast (B, a subset of *Data 3*) and as functions of logarithm of luminance (C, a subset of *Data 1* and *Data 5*). Colors denote the experimental conditions (see figure legends).

by Watson and Solomon (1997), first applying linear filters (using the OTF and the NTF) and then applying the nonlinear neuronal response (f). Hence, f is a function of contrast values that are lower than the actual stimulus contrast and the c_{50} model parameter could be lower than c_{50} measurements reported in individual cells.

In addition to our preference for presenting a simple model, our choice to model acuity with a single visual channel was informed by the findings of Majaj, Pelli, Kurshan, and Palomares (2002), who concluded that letters are identified using a single channel that matches their size. We considered this finding to be an experimental validation of linear models that use template images of adapted sizes for letter recognition, such as the one presented here and in our previous work (Leroux et al., 2024). Watson and Ahumada (2012) also developed a single-channel model to predict visual acuity, whereas Nestares et al. (2003) used multiple channels to predict acuity measurements. The benefit of modeling acuity using multiple channels remains to be demonstrated. On the one hand, it offers greater degrees of freedom, which, in turn, can improve model predictions. On the other hand, the existence of multiple visual channels has been primarily revealed by experiments using narrowband stimuli (Blakemore & Campbell, 1969; Campbell & Robson, 1968; Graham & Nachmias, 1971), unlike in acuity testing.

The effect of stimulus contrast on acuity is illustrated in Fig. 3B, which shows a dramatic loss of visual acuity at the lowest values of stimulus contrast. This graph, originally presented by Johnson and Casson (see Figure 4 in their study), inspired us to account for neuronal nonlinearity in the acuity model. Our results confirmed that neuronal nonlinearity can explain Johnson and Casson's observations. Neglecting the nonlinearity resulted in a much weaker dependency of visual acuity on stimulus contrast (dashed lines in Fig. 3B). Other studies corroborated Johnson and Casson's findings, reporting an approximately 0.3 logMAR acuity improvement when stimulus contrast increases from 10% to 100% (Abadi & Pantazidou, 1996; Brown & Lovie-Kitchin, 1989; Elliott & Bullimore, 1993; Lovie-Kitchin & Brown, 2000), with a steeper improvement bellow 10% (Abadi & Pantazidou, 1996). Unfortunately, many published studies did not specify the type of stimulus contrast (Michelson or Weber), resulting in an ambiguity of a factor of two in the limit of low contrast and making precise quantitative comparisons between studies difficult.

Neglecting neuronal nonlinearity also offsets the curve of predicted acuity loss as luminance decreases, relative to measurements, in a contrast-dependent manner. The slopes of measurements and models remain similar, on the order of approximately 0.15 logMAR per log luminance. According to the review by Wood et al. (2021), those rates are higher than the typical values (0.06 to 0.14 logMAR per log luminance) reported in healthy subjects at higher nominal luminance (160 cd/m^2 on average). The discrepancy likely originates from the saturation of visual acuity above 200 cd/m^2 (Rabin, 1994; Sheedy, Bailey, & Raasch, 1984).

Conclusion

We have developed a simple model that accurately predicts subject-averaged acuity measurements over extended ranges of stimulus contrast, luminance, and blur. We have demonstrated that neuronal nonlinearity is essential to modeling acuity in these non-standard conditions, using a relatively small number of fit parameters: two for nonlinearity, and three for the four luminance levels. Our approach is an interesting tradeoff between complexity and applicability, and may help in interpreting clinical data involving low-contrast or low-luminance visual acuity.

CRediT authorship contribution statement

Charles-Edouard Leroux: Writing – review & editing, Writing – original draft, Visualization, Software, Methodology, Investigation, Formal analysis, Data curation, Conceptualization. **Christophe Fontvieille:** Writing – review & editing, Writing – original draft, Validation, Supervision, Methodology. **Fabrice Bardin:** Writing – review & editing, Writing – original draft, Visualization, Validation, Supervision, Project administration, Methodology, Investigation, Funding acquisition, Formal analysis, Data curation, Conceptualization.

References

Abadi, R. V., & Pantazidou, M. (1996). Low contrast letter acuity in age-related maculopathy. *Ophthalmic & Physiological Optics*, *16*(6), 455–459. http://dx.doi.org/10.1016/0275-5408(96)00012-9.

Albrecht, D. G., & Hamilton, D. B. (1982). Striate cortex of monkey and cat: contrast response function. *Journal of Neurophysiology*, *48*(1), 217–237. http://dx.doi.org/10.1152/jn.1982.48.1.217.

Applegate, R. A., Marsack, J. D., & Thibos, L. N. (2006). Metrics of retinal image quality predict visual performance in eyes with 20/17 or better visual acuity. *Optometry and Vision Science*, *83*(9), 635. http://dx.doi.org/10.1097/01.opx.0000232842.60932.af.

Baier, M., Cutter, G., Rudick, R., Miller, D., Cohen, J., Weinstock-Guttman, B., et al. (2005). Low-contrast letter acuity testing captures visual dysfunction in patients with multiple sclerosis. *Neurology*, *64*(6), 992–995. http://dx.doi.org/10.1212/01.WNL.0000154521.40686.63.

Barrett, H. H., & Myers, K. J. (2003). *Foundations of image science*. John Wiley & Sons.

Blakemore, C., & Campbell, F. W. (1969). On the existence of neurones in the human visual system selectively sensitive to the orientation and size of retinal images. *The Journal of Physiology*, *203*(1), 237–260. http://dx.doi.org/10.1113/jphysiol.1969.sp008862.

Brown, B., & Lovie-Kitchin, J. E. (1989). High and low contrast acuity and clinical contrast sensitivity tested in a normal population. *Optometry and Vision Science*, *66*(7), 467–473. http://dx.doi.org/10.1097/00006324-198907000-00010.

Buehren, T., & Collins, M. J. (2006). Accommodation stimulus–response function and retinal image quality. *Vision Research*, *46*(10), 1633–1645. http://dx.doi.org/10.1016/j.visres.2005.06.009.

Campbell, F. W., & Robson, J. G. (1968). Application of Fourier analysis to the visibility of gratings. *Journal of Physiology*, *197*(3), 551–566. http://dx.doi.org/10.1113/jphysiol.1968.sp008574.

Carandini, M., & Heeger, D. J. (1994). Summation and division by neurons in primate visual cortex. *Science*, *264*(5163), 1333–1336. http://dx.doi.org/10.1126/science.8191289.

Carandini, M., Heeger, D. J., & Movshon, J. A. (1997). Linearity and normalization in simple cells of the macaque primary visual cortex. *Journal of Neuroscience*, *17*(21), 8621–8644. http://dx.doi.org/10.1523/JNEUROSCI.17-21-08621.1997.

Dalimier, E., & Dainty, C. (2008). Use of a customized vision model to analyze the effects of higher-order ocular aberrations and neural filtering on contrast threshold performance. *Journal of the Optical Society of America A*, *25*(8), 2078–2087. http://dx.doi.org/10.1364/JOSAA.25.002078.

Dalimier, E., Dainty, C., & Barbur, J. L. (2008). Effects of higher-order aberrations on contrast acuity as a function of light level. *Journal of Modern Optics*, *55*(4–5), 791–803. http://dx.doi.org/10.1080/09500340701469641.

Duong, T., & Freeman, R. D. (2008). Contrast sensitivity is enhanced by expansive nonlinear processing in the lateral geniculate nucleus. *Journal of Neurophysiology*, *99*(1), 367–372. http://dx.doi.org/10.1152/jn.00873.2007.

Elliott, D. B., & Bullimore, M. A. (1993). Assessing the reliability, discriminative ability, and validity of disability glare tests. *Investigative Ophthalmology & Visual Science*, *34*(1), 108–119.

Graham, N., & Nachmias, J. (1971). Detection of grating patterns containing two spatial frequencies: A comparison of single-channel and multiple-channels models. *Vision Research*, *11*(3), 251–259. http://dx.doi.org/10.1016/0042-6989(71)90189-1.

Guirao, A., & Williams, D. R. (2003). A method to predict refractive errors from wave aberration data. *Optometry and Vision Science*, *80*(1), 36–42. http://dx.doi.org/10.1097/00006324-200301000-00006.

Hastings, G. D., Marsack, J. D., Thibos, L. N., & Applegate, R. A. (2020). Combining optical and neural components in physiological visual image quality metrics as functions of luminance and age. *Journal of Vision*, *20*(7), 20. http://dx.doi.org/10.1167/JOV.20.7.20.

Johnson, C. A., & Casson, E. J. (1995). Effects of luminance, contrast, and blur on visual acuity. *Optometry and Vision Science*, *72*, 864–869. http://dx.doi.org/10.1097/00006324-199512000-00004.

Kilintari, M., Pallikaris, A., Tsiklis, N., & Ginis, H. S. (2010). Evaluation of image quality metrics for the prediction of subjective best focus. *Optometry and Vision Science*, *87*(3), 183–189. http://dx.doi.org/10.1097/OPX.0b013e3181cdde32.

Leroux, C.-E., Leahy, C., Dupuis, J., Fontvieille, C., & Bardin, F. (2024). Defining metrics of visual acuity from theoretical models of observers. *Journal of Vision*, *24*(4), 14. http://dx.doi.org/10.1167/jov.24.4.14.

López-Gil, N., Martin, J., Liu, T., Bradley, A., Díaz-Muñoz, D., & Thibos, L. N. (2013). Retinal image quality during accommodation. *Ophthalmic & Physiological Optics*, *33*(4), 497–507. http://dx.doi.org/10.1111/opo.12075.

Lovie-Kitchin, J. E., & Brown, B. (2000). Repeatability and intercorrelations of standard vision tests as a function of age. *Optometry and Vision Science*, *77*(8), 412–420. http://dx.doi.org/10.1097/00006324-200008000-00008.

Majaj, N. J., Pelli, D. G., Kurshan, P., & Palomares, M. (2002). The role of spatial frequency channels in letter identification. *Vision Research*, *42*(9), 1165–1184. http://dx.doi.org/10.1016/S0042-6989(02)00045-7.

Marcos, S., Sawides, L., Gambra, E., & Dorronsoro, C. (2008). Influence of adaptive-optics ocular aberration correction on visual acuity at different luminances and contrast polarities. *Journal of Vision*, *8*(13), 1. http://dx.doi.org/10.1167/8.13.1.

Martin, J., Vasudevan, B., Himebaugh, N., Bradley, A., & Thibos, L. (2011). Unbiased estimation of refractive state of aberrated eyes. *Vision Research*, *51*(17), 1932–1940. http://dx.doi.org/10.1016/j.visres.2011.07.006.

Nestares, O., Navarro, R., & Antona, B. (2003). Bayesian model of snellen visual acuity. *Journal of the Optical Society of America A*, *20*(7), 1371–1381. http://dx.doi.org/10.1364/JOSAA.20.001371.

Pesudovs, K., Marsack, J. D., Donnelly, W. J., Thibos, L. N., & Applegate, R. A. (2004). Measuring visual acuity-mesopic or photopic conditions, and high or low contrast letters? *Journal of Refractive Surgery*, *20*(5), http://dx.doi.org/10.3928/1081-597X-20040901-20.

Rabin, J. (1994). Luminance effects on visual acuity and small letter contrast sensitivity. *Optometry and Vision Science*, *71*(11), 685–688. http://dx.doi.org/10.1097/00006324-199411000-00003.

Rathbun, D. L., Alitto, H. J., Warland, D. K., & Usrey, W. M. (2016). Stimulus contrast and retinogeniculate signal processing. *Frontiers in Neural Circuits*, *10*, 8. http://dx.doi.org/10.3389/fncir.2016.00008.

Roorda, A., Cholewiak, S. A., Bhargava, S., Ivzan, N. H., LaRocca, F., Nankivil, D., et al. (2023). The visual benefits of correcting longitudinal and transverse chromatic aberration. *Journal of Vision*, *23*(2), 3. http://dx.doi.org/10.1167/jov.23.2.3.

Scholl, B., Latimer, K. W., & Priebe, N. J. (2012). A retinal source of spatial contrast gain control. *Journal of Neuroscience*, *32*(29), 9824–9830. http://dx.doi.org/10.1523/JNEUROSCI.0207-12.2012.

Sheedy, J. E., Bailey, I. L., & Raasch, T. W. (1984). Visual acuity and chart luminance. *Optometry and Vision Science*, *61*(9), 595–600. http://dx.doi.org/10.1097/00006324-198409000-00010.

Tarrant, J., Roorda, A., & Wildsoet, C. F. (2010). Determining the accommodative response from wavefront aberrations. *Journal of Vision*, *10*(5), 4. http://dx.doi.org/10.1167/10.5.4.

Thibos, L. N. (2009). Retinal image quality for virtual eyes generated by a statistical model of ocular wavefront aberrations. *Ophthalmic & Physiological Optics*, *29*(3), 288–291. http://dx.doi.org/10.1111/j.1475-1313.2009.00662.x.

Thibos, L. N., Hong, X., Bradley, A., & Applegate, R. A. (2004). Accuracy and precision of objective refraction from wavefront aberrations. *Journal of Vision*, *4*(4), 9. http://dx.doi.org/10.1167/4.4.9.

Villegas, E. A., Alcón, E., & Artal, P. (2008). Optical quality of the eye in subjects with normal and excellent visual acuity. *Investigative Ophthalmology and Visual Science*, *49*(10), 4688–4696. http://dx.doi.org/10.1167/iovs.08-2316.

Watson, A. B., & Ahumada, A. J. (2005). A standard model for foveal detection of spatial contrast. *Journal of Vision*, *5*(9), 6. http://dx.doi.org/10.1167/5.9.6.

Watson, A. B., & Ahumada, A. J. (2008). Predicting visual acuity from wavefront aberrations. *Journal of Vision*, *8*(4), 17. http://dx.doi.org/10.1167/8.4.17.

Watson, A. B., & Ahumada, A. J. (2012). Modeling acuity for optotypes varying in complexity. *Journal of Vision*, *12*(10), 19. http://dx.doi.org/10.1167/12.10.19.

Watson, A. B., & Ahumada, A. J. (2015). Letter identification and the neural image classifier. *Journal of Vision*, *15*(2), 15. http://dx.doi.org/10.1167/15.2.15.

Watson, A. B., & Solomon, J. A. (1997). Model of visual contrast gain control and pattern masking. *Journal of the Optical Society of America A*, *14*(9), 2379–2391. http://dx.doi.org/10.1364/JOSAA.14.002379.

Watson, A. B., & Yellott, J. I. (2012). A unified formula for light-adapted pupil size. *Journal of Vision*, *12*(10), 12. http://dx.doi.org/10.1167/12.10.12.

Wood, L. J., Jolly, J. K., Buckley, T. M., Josan, A. S., & MacLaren, R. E. (2021). Low luminance visual acuity as a clinical measure and clinical trial outcome measure: a scoping review. *Ophthalmic & Physiological Optics*, *41*(2), 213–223. http://dx.doi.org/10.1111/opo.12775.

Yi, F., Iskander, D. R., & Collins, M. (2011). Depth of focus and visual acuity with primary and secondary spherical aberration. *Vision Research*, *51*(14), 1648–1658. http://dx.doi.org/10.1016/j.visres.2011.05.006.

Zheleznyak, L., Jung, H., & Yoon, G. (2014). Impact of pupil transmission apodization on presbyopic through-focus visual performance with spherical aberration. *Investigative Ophthalmology and Visual Science*, *55*(1), 70–77. http://dx.doi.org/10.1167/iovs.13-13107.

Zheleznyak, L., Sabesan, R., Oh, J.-S., MacRae, S., & Yoon, G. (2013). Modified monovision with spherical aberration to improve presbyopic through-focus visual performance. *Investigative Ophthalmology and Visual Science*, *54*(5), 3157–3165. http://dx.doi.org/10.1167/iovs.12-11050.